Journal of Cancer Research and Clinical Oncology (2019) 145:373–381
https://doi.org/10.1007/s00432-018-2798-y

ORIGINAL ARTICLE – CANCER RESEARCH

Spatiotemporal characteristics of fibroblasts-dependent cancer cell invasion

Tomoyuki Miyashita[1,2] · Tomokazu Omori[2,3] · Hiroshi Nakamura[2,4] · Masato Sugano[2,4] · Shinya Neri[2] · Satoshi Fujii[2] · Hiroko Hashimoto[2] · Masahiro Tsuboi[3] · Atsushi Ochiai[1,5] · Genichiro Ishii[1,2]

Received: 7 August 2018 / Accepted: 16 November 2018 / Published online: 23 November 2018

Abstract

Purpose Cancer cells can invade the surrounding stroma with the aid of fibroblasts (fibroblasts-dependent invasion). The aim of this study was to explore the spatiotemporal characteristics of fibroblast-dependent invasion of cancer cells.

Methods We performed an in vitro three-dimensional collagen invasion assay using Fluorescent Ubiquitination-based Cell Cycle indicator (Fucci)-labeled A431 carcinoma cells co-cultured with fibroblasts. We used time-lapse imaging to analyze the total cell number, frequencies of small cancer cell nests and S/G2/M phase of A431 cells in the invasion area. We compared the frequencies of small cancer cell nests and geminin (+) cancer cells within fibroblast-rich areas and fibroblast-poor areas in surgically resected human invasive squamous cell carcinoma tissue.

Results The total invasion number of A431 cells was significantly higher when cultured with fibroblasts than without. The formation of small cancer cell nests was observed within the invasion area only in the presence of fibroblasts. The frequency of S/G2/M phase cells was significantly higher in A431 cells when cultured with fibroblasts than without. Immunohistochemical analysis of surgically resected human invasive squamous cell carcinoma tissue revealed that the frequencies of small cancer cell nests and geminin-positive cancer cells were significantly higher in fibroblast-rich areas compared to those in fibroblast-poor areas within the same tumor region.

Conclusion Our current study clearly showed that fibroblast-dependent cancer cell invasion was characterized by the progression in cell cycle and formation of small cancer cell nests.

Keywords Squamous cell carcinoma · Fucci · Cell cycle · Invasion · Fibroblasts

Electronic supplementary material The online version of this article (https://doi.org/10.1007/s00432-018-2798-y) contains supplementary material, which is available to authorized users.

✉ Genichiro Ishii
gishii@east.ncc.go.jp

1 Laboratory of Cancer Biology, Department of Integrated Biosciences, Graduate School of Frontier Sciences, The University of Tokyo, Kashiwa, Chiba, Japan

2 Division of Pathology, Exploratory Oncology Research and Clinical Trial Center, National Cancer Center, 6-5-1, Kashiwanoha, Kashiwa 277-8577, Chiba, Japan

3 Division of Thoracic Surgery, National Cancer Center Hospital East, Kashiwa, Chiba, Japan

4 Department of Pathology and Clinical Laboratories, National Cancer Center Hospital East, Kashiwa, Japan

5 Exploratory Oncology Research and Clinical Trial Center, National Cancer Center, Kashiwa, Chiba, Japan

Abbreviations

CAFs	Cancer-associated fibroblasts
DMEM	Dulbecco's modified Eagle's medium
ECM	Extracellular matrix
Fucci	Fluorescent ubiquitination-based cell cycle indicator
HRP	Horseradish peroxidase
MMP	Matrix metalloproteinase

Introduction

During metastasis, cancer cells penetrate the basement membrane and invade the stroma to reach blood or lymph vessels, from where they can be carried to other organs (Schroeder et al. 2011; Sahai 2007; Clark and Vignjevic 2015). Cancer stroma, which is the path of invading cancer cells, is characterized by a high number of fibroblasts and an extracellular matrix (ECM) primarily made up of collagen type I

(Kalluri and Zeisberg 2006). Previous in vitro and in vivo studies have revealed diverse mechanisms by which cancer cells invade into the stroma (Friedl and Alexander 2011; Friedl et al. 2012). Single-cell invasion is characterized by a lack of cell–cell interactions (Lammermann and Sixt 2009; Madsen and Sahai 2010; Wolf et al. 2003). Some studies have also shown that the cells causing single-cell invasion have a mesenchymal cell-like phenotype, which is characterized by a spindle-shaped cell body (Wolf et al. 2007; Friedl and Wolf 2009; Sanz-Moreno et al. 2008). On the contrary, collective invasion is characterized by groups of cells that retain cell–cell adhesion (Khalil and Friedl 2010; Konen et al. 2017; Labernadie et al. 2017). The interplay between intrinsic factors of cancer cells themselves and extrinsic stromal factors, such as fibroblasts- and ECM-derived factors, affect the cancer cell invasion (Skhinas and Cox 2017).

Stromal components provide a specialized microenvironment for cancer cell proliferation and invasion. Cancer–associated fibroblasts (CAFs) are the most abundant component in the cancer stroma and can influence local invasion of cancer cells via several biochemical and biomechanical factors. Previous studies have indicated that biomechanical remodeling of the ECM by CAFs can facilitate cancer cell invasion into the matrix with the aid of the CAFs (Gaggioli et al. 2007; Neri et al. 2015, 2016, 2017). This type of cancer cell invasion might be affected not only by the properties of cancer cells themselves, such as proteases and Rho function but also by the properties of CAFs. We recently reported that podoplanin-expressing CAFs favor the local invasion of cancer cells via the increase in remodeled areas of the ECM (Neri et al. 2015). These findings suggest that the capacity of CAFs to remodel the ECM influences the number of invading cancer cells.

Human pathological studies have revealed a great diversity in stromal components. For example, for lung adenocarcinoma, scirrhous-type gastric adenocarcinoma, and pancreatic adenocarcinoma, it is well-known that the tumor stroma is abundantly composed of CAFs and ECM. On the other hand, in the stroma of malignant lymphoma and melanoma, the number of CAFs is relatively small. Even within the same tumor, there are fibroblast-rich and fibroblast-poor areas. Therefore, it is of great interest to reveal the biological characteristics of invading cancer cells associated with fibroblast.

To elucidate this in more detail, three-dimensional time-lapse analysis was required. In the current study, we used cancer cells with Fucci (fluorescent ubiquitination-based cell cycle indicator) system (Sakaue-Sawano et al. 2011; Miyashita et al. 2017). These Fucci-labeled cancer cells were cultured either in the presence or in the absence of fibroblasts. Then, using time-lapse imaging technique for in vitro three-dimensional collagen invasion assay, we evaluated the total invasion number, morphological pattern of cancer cell nests, frequency of apoptosis (apoptotic bodies/invaded cells), and frequency of the S/G2/M phase of invading cancer cells in collagen type I.

Materials and methods

Cell culture

The human squamous cell carcinoma line A431 was obtained from the ATCC (American Type Culture Collection, Manassas, VA). A431 cells were cultured in Dulbecco's modified Eagle's medium (DMEM) from Sigma (St. Louis, MO) supplemented with 10% FBS (fetal bovine serum, Sigma), and 1% penicillin and streptomycin (Sigma). Cells were incubated at 37 °C in an atmosphere containing 5% CO2. The human foreskin fibroblast was obtained from CET (Cellular Engineering Technologies, Coralville, IA). Fibroblast was cultured in minimum essential medium Eagle, alpha modification (α-MEM) (Sigma) supplemented with 10% fetal bovine serum, 1% penicillin and streptomycin. Cells were incubated at 37 °C in an atmosphere containing 5% CO2.

Collagen invasion assay

Cancer cells used for the collagen invasion assay were Fucci transfected cells established previously (Fucci-encoding vector was kindly provided from Dr. Miyawaki of the RIKEN Brain Science Institute) (Miyashita et al. 2017). Either the cancer cells alone or a mixed population of human foreskin fibroblasts and cancer cells were plated on collagen-coated (0.3% collagen type I gel; Nitta Gelatin, Osaka, Japan) Essen ImageLock 96-well plates (Essen BioScience, Ann Arbor, MI), at a density of either 1×10^5 cancer cells/well, or 5×10^4 human foreskin fibroblasts and cancer cells/well. After an incubation period of 1 h, a wound was made in the cell layer using the 96-well WoundMaker (Essen BioScience), and the cells were embedded in collagen type I gel (Nitta Gelatin). Fresh medium was added and images of scratched field were then obtained using the IncuCyte Live-Cell Imaging System (Essen BioScience). Time-lapse fluorescence and phase-contrast images were obtained at 3-h intervals for 72 h. Each data element was measured for at least five fields (magnification × 10) in three independent experiments.

Image analysis

Image analysis was performed as previously described (Neri et al. 2016, 2017). Briefly, algorithms were developed to evaluate the observations of each experiment as follows:

1. The invasion region was detected using the first frame of the phase contrast images.
2. The number of invaded cancer cells was determined based on Fucci fluorescence.
3. The growth rate of invaded cancer cells was determined based on green and red fluorescence.
4. The cell death ratio was calculated by the following formula at 72 h. The apoptotic bodied was detected by Caspase-3/7 apoptosis reagent (Essen BioScience).

$$[\text{The cell death ratio}] = [\text{The number of apoptotic bodies}] / [\text{The number of invaded cancer cells}].$$

Pathological studies

We enrolled 14 patients with peripheral squamous cell carcinoma of the lung measuring 30 mm or less in diameter that were surgically resected at the National Cancer Center Hospital East between February 2004 and December 2013 (supplemental Table 1). We selected peripheral squamous cell carcinoma of the lung, since peripheral SCC composed of alveolar space filling area (Fibroblast-poor area) and alveolar space destructing area (fibroblast-rich area) and it is easy to discriminate between two areas (Funai et al. 2003). All surgical specimens were collected and analyzed after receiving approval from the Institutional Review Board of the National Cancer Center Hospital East (IRB number 2017-158).

Surgical specimens were fixed with 10% formalin and embedded in paraffin. The tumors were cut at approximately 5-mm intervals, and serial 3-μm sections were stained with hematoxylin and eosin. In this study, we defined the fibroblast-rich and fibroblast-poor areas according to the following criteria:

1. *Fibroblast-rich area* The tumor cells form irregular-shaped nests, intermingled with an extensive stroma.
2. *Fibroblast-poor area* The tumor cells show growth by filling the alveolar space separated by thin preexisting septa. Desmoplastic stroma is not found within this component (Funai et al. 2003).

Immunohistochemistry

Immunostaining was performed using 4-μm paraffin-embedded serial tissue sections. The slides were deparaffinized in xylene and rehydrated in graded ethanol. After antigen-retrieval, individual slides were incubated overnight at 4 °C using mouse monoclonal antibody Geminin (Leica, Wetzlar, Germany) at a final dilution of 1:40. We used Fucci transfected cells in in vitro experiments and analyzed the cell cycle status based on green fluorescent of Fucci (mVenus-hGeminin). In order to be consistent with the results from in vitro experiments, we used geminin antibody in surgical materials. After washing with PBS, the slides were incubated with EnVision + System-HRP Labeled Polymer Anti-mouse (Agilent, Santa Clara, CA) for 1 h at room temperature. After washing with PBS, the color reaction using HRP was performed for 3 min in 2% 3, 3′-diaminobenzidine in 50 mM Tris-buffer (pH 7.6) containing 0.3% hydrogen peroxidase. Finally, the sections were counterstained with Meyer's hematoxylin, dehydrated, and mounted.

Evaluation of the frequency of small cancer cell nests in surgically resected specimens

In this study, we defined small cancer cell nests as less than 5000 μm^2 (the number of cancer cells within a nest was about 25–50). After acquiring whole slide image by slide scanner (NanoZoomer Digital Pathology virtual slide viewer, Hamamatsu Photonics, Shizuoka, Japan), we randomly selected fields (1.5 mm^2/field) within the fibroblast-rich area and the fibroblast-poor area, and we measured at least ten nests in each area. The frequency of small cancer cell nests was evaluated by the following formula.

$$[\text{The frequency of small cancer cell nests}] = [\text{The number of small cancer cell nests}] / [\text{The number of total cancer cell nests}].$$

Evaluation of the frequency of geminin-positive cancer cells

Using the whole slide image, we randomly selected five fields within both fibroblast-rich and fibroblast-poor areas. The frequency of geminin-positive cancer cells was evaluated in these fields (0.1 mm^2) for each area. The ratio of the geminin-positive cancer cells per field was measured and average number was used as the ratio of the geminin-positive cancer cells in each case.

Statistical analysis

Statistical significance was assessed by the Student's *t* test. Comparison between fibroblasts-rich area and fibroblast-poor area was assessed by the Wilcoxon signed-rank test. *p* values of <0.05 were considered statistically significant.

Results

Fibroblasts enhanced cancer cell invasion into the collagen matrix

We examined the number of A431 cells which invaded the ECM every 12 h. After 72 h, the total number of A431 cells in the invasion area was evaluated (Fig. 1a, b). When co-cultured with fibroblasts, the total number of A431 cells in the invasion area was 321.2 ± 57.1, whereas the number of invaded A431 cells was 44.9 ± 23.1 when A431 cells were seeded alone ($p < 0.01$). The number of invaded A431 cells, when co-cultured with fibroblasts, was significantly higher than that of A431 cells alone at all time points (Fig. 1c). In this collagen invasion assay, we observed that human foreskin fibroblasts extensively invaded the collagen matrix, and furthermore, the cancer cells followed the leading human foreskin fibroblasts and invaded (fibroblast-dependent cancer cell invasion).

Next, we measured the maximum distance of invasion. The maximum distance of invasion measured for A431 cells co-cultured with fibroblasts was significantly larger than that measured for A431 cells alone (206.8 ± 15.3 μm vs. 46.2 ± 17.0 μm, $p < 0.01$) (Fig. 2a, b).

Fibroblasts increased the frequency of S/G2/M phase in A431 cells invading into the collagen matrix

Cell cycle status of A431-Fucci cells within invasion area was analyzed (Supplemental Fig. 2a, b). Representative images of A431-Fucci cells at 72 h are shown in Fig. 3a (fibroblasts-absent) and Fig. 3b (fibroblasts-present). Although the frequency of invaded A431 cells with green fluorescence (with S/G2/M phase) was not significantly different between the two groups until first 48 h. However, the frequency of green fluorescent cells was higher in A431 cells co-cultured with fibroblasts compared to A431 cells alone at 60 h (30.0 ± 3.5% vs. 24.3 ± 2.5%, $p < 0.1$) and 72 h (28.8 ± 4.3% vs. 21.1 ± 1.5%, $p < 0.05$) (Fig. 3c).

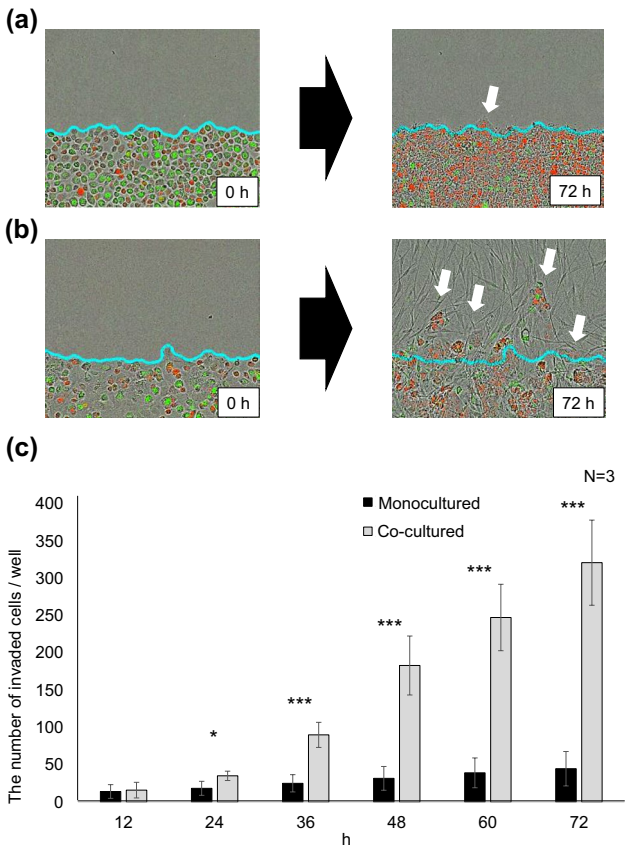

Fig. 1 Total number of invaded A431 cells in the invasion area. **a** Representative image of invaded A431 cells in monoculture. White arrow indicates the invasion point. **b** Representative image of cancer cells co-cultured with fibroblasts. White arrow indicates the invasion point. **c** The average number of invaded A431 cells evaluated every 12 h. Values are given as mean ± SD from three independent experiments. Statistical analysis was performed using Student's *t* test. *$p < 0.1$, ***$p < 0.01$

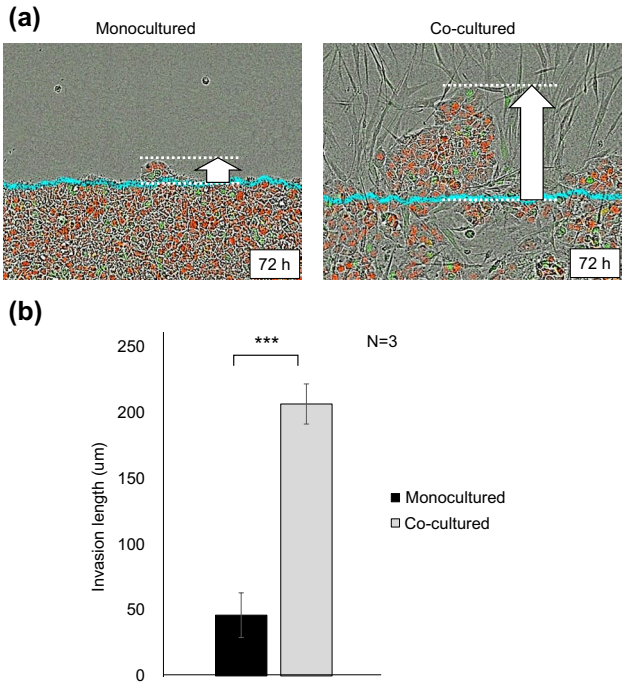

Fig. 2 The maximum distance of invasion by A431 cells. **a** Representative image of the maximum invasion distance of A431 cells in monoculture or when co-cultured with fibroblasts at 72 h. Left panel: monoculture. Right panel: co-cultured with fibroblasts. Blue line: initial scratch line. White arrow: maximum invasion distance. **b** The average maximum invasion distance at 72 h. Values are given as mean ± SD from three independent experiments. Statistical analysis was performed using Student's *t* test. ***$p < 0.01$

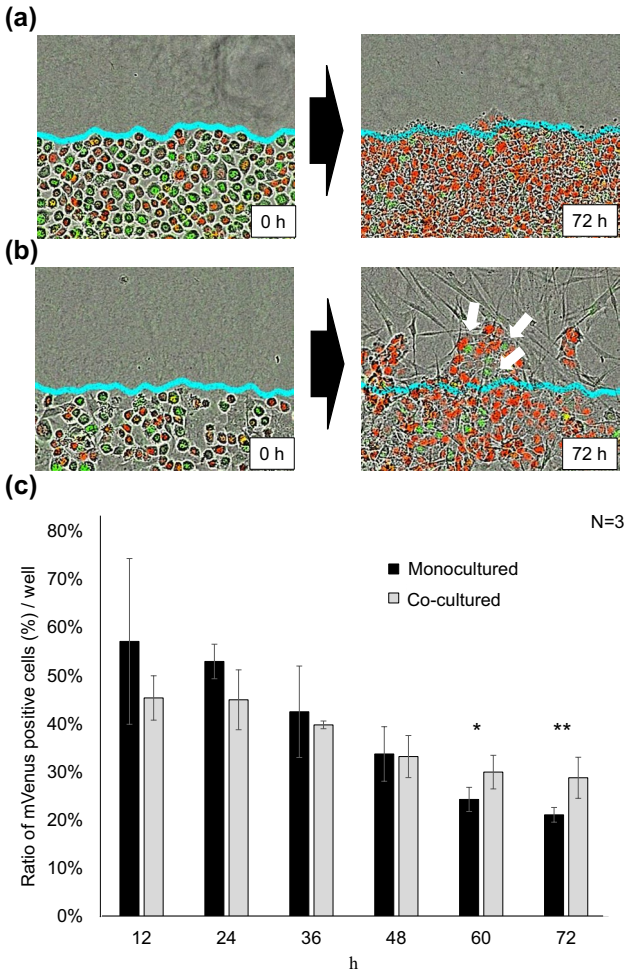

Fig. 3 Frequency of S/G2/M phase in invaded A431 cells. **a** Representative image of cell cycle progression of invaded A431 cells in monoculture. **b** Representative image of cell cycle progression of invaded A431 cells when co-cultured with fibroblasts. White arrow indicates the invaded cells with green fluorescence. **c** The average ratio of S/G2/M phase in invaded A431 cells at every 12 h. Values are provided as mean ± SD from three independent experiments. Statistical analysis was performed using Student's *t* test. $*p < 0.1$, $**p < 0.05$

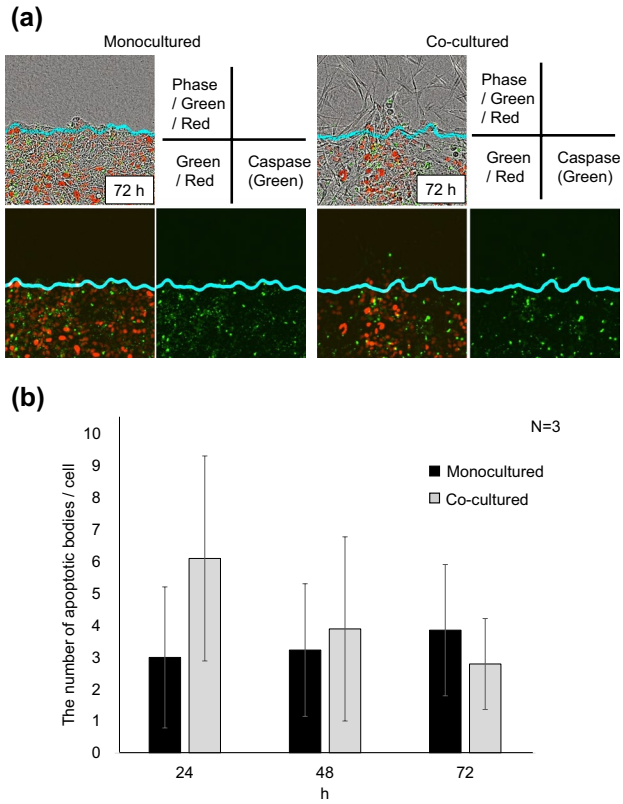

Fig. 4 Apoptotic ratio of invaded A431 cells. **a** Representative image of invaded A431 cells in monoculture (left panels) and when co-cultured with fibroblasts (right panels) at 72 h. Red fluorescence: mCherry-hCdt1. Green fluorescence: nuclei of caspase 3/7 activated cells, **b** calculated apoptotic ratios. Values are given as mean ± SD from three independent experiments. Statistical analysis was performed using Student's *t* test

Apoptotic ratio of A431 cells invaded into collagen matrix

To calculate the apoptotic cell ratio of invaded A431 cells, we used A431-mCherry-hCdt1 cells, the fluorescence of which indicated the G0/G1 phase of the cell. Representative images of apoptotic cells at 72 h are shown in Fig. 4a (left: fibroblast-absent, right: fibroblast-present). The green fluorescence corresponded with the nuclei of caspase-activated cells (see also material and methods). There was no significant difference in the apoptotic ratio of invaded A431 cells between the two groups (Fig. 4b).

Characteristic cancer cell nest of A431 cells invaded into collagen matrix

Within the invasion area, A431 cells formed cancer cell nests showing heterogeneous morphology. We classified these nests into the following three patterns: Type (A) Cancer cell nest continuously connected from the start of the line, Type (B) Cancer cell nest separated from the start of the line and containing more than six cells, and Type (C) Cancer cell nest separated from the start of the line and containing less than 5 cells (Fig. 5a). Representative images of type A, B, and C nests at 72 h are shown in the left panel (fibroblast-absent) and the right panel (fibroblasts-present) of Fig. 5b. When A431 cells were alone, the number of type A pattern was 1.9 ± 0.9/well. On the contrary, type B and C patterns were not found at all. When A431 cells were cultured with fibroblasts, the number of type A, type B, and type C patterns was 7.3 ± 0.5/well, 1.5 ± 0.5/well, and 3.5 ± 2.7/well, respectively (Fig. 5c). It is noteworthy that type B and type C patterns were detected only when fibroblasts coexist with

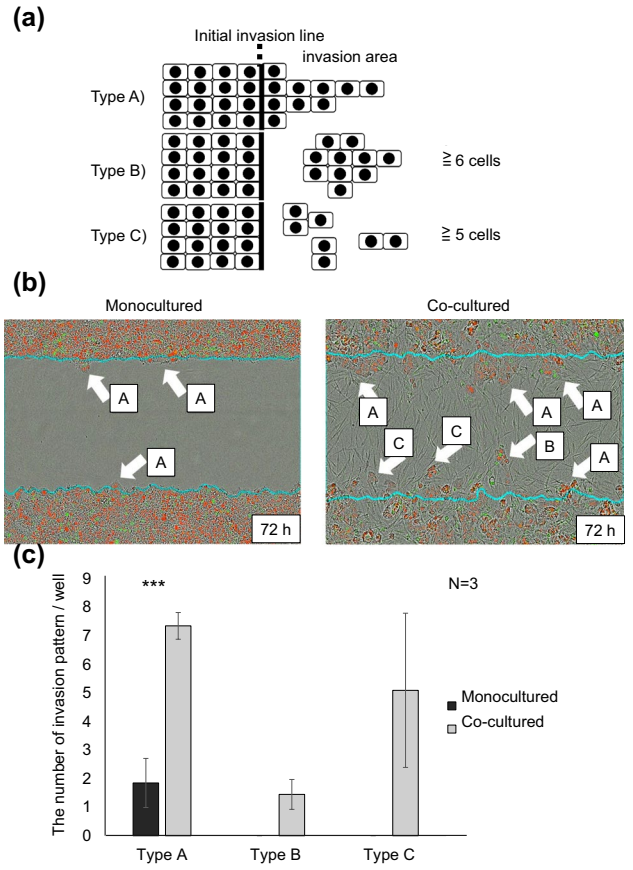

Fig. 5 Morphological classification of cancer cell nest. **a** Three morphological patterns of cancer cell nests (Type A, B, and C). **b** Representative image of morphological patterns of invaded A431 cells in monoculture (left panels) and when co-cultured with fibroblasts (right panels) at 72 h. **c** The number of invasion patterns. Values are provided as mean ± SD from three independent experiments. Statistical analysis was performed using Student's *t* test. ***$p < 0.01$

A431 cells. Cancer cell nests with the type C pattern exhibit the histological morphology of "tumor budding" which is often found on the invasive front of several cancers.

Squamous cell carcinoma cells within fibroblast-rich area display higher frequency of small cancer cell nest and higher proliferation activity

To confirm whether the results obtained from in vitro experiments could be reproduced in in vivo conditions, we used surgically resected peripheral small human lung squamous cell carcinoma tissues. The blue square in Fig. 6a shows the central area where cancer cells and abundant cancer-associated fibroblasts are intermingled (fibroblast-rich area). On the other hand, the red square indicates the peripheral region of cancer in which cancer cells mainly display alveolar space filling growth (Funai et al. 2003) and contain less stromal cells (fibroblast-poor area). We compared the proliferation index of cancer cells within fibroblast-rich area and fibroblast-poor area. Representative images of fibroblast-rich and fibroblast-poor areas are shown in Fig. 6a. The ratio of geminin-positive cancer cells was significantly higher in fibroblasts-rich areas than in fibroblasts-poor areas within the same tumor ($p < 0.01$) (Fig. 6b). Moreover, we compared the number of small cancer cell nests (containing less than 50 cancer cells) within fibroblasts-rich area and fibroblasts-poor area (Fig. 6c) within the same tumor. Small cancer cell nests were found more often in fibroblast-rich areas than in fibroblasts-poor areas ($p < 0.01$) (Fig. 6d).

Discussion

During the metastatic process, cancer cells invade the stroma, which is characterized by the recruited fibroblasts and deposited ECM, including collagen type I. The fibroblasts and ECM can influence local invasion of cancer cells by several biochemical and biomechanical mechanisms (Friedl and Wolf 2003; Ishii et al. 2016). Human pathology studies have revealed a great diversity in the stromal components among several types of cancer. Moreover, even within the same tumor, there are fibroblast-rich areas as well as fibroblast-poor areas. By using a time-lapse imaging technique for in vitro three-dimensional invasion model, we first revealed the following characteristics of cancer cells invading into collagen matrix: (1) cancer cells showed greater extent of invasion into collagen type I in the presence of fibroblasts, (2) small cancer cell nests were observed only when fibroblasts were present, and (3) the frequency of proliferating cancer cells in the invasion area was significantly higher when they were co-cultured with fibroblasts. These results may indicate direct rationale for the heterogeneity of fibrous microenvironment and provide key information on how this heterogeneity affects biological diversity of invading cancer cells.

CAFs-mediated mechanisms that stimulate cancer cell invasion have been previously reported. Gaggioli et al. (2007) have studied one such mechanism in which CAFs facilitate the local invasion of cancer cells by physically remodeling the extracellular matrix. They revealed that generation of tracks by fibroblasts is sufficient to enable the collective invasion of the squamous cell carcinoma cells. We have also previously demonstrated that CAFs expressing podoplanin invaded a collagen matrix to a greater extent and enhanced the local invasion of cancer cells via a similar mechanism and suggested the possibility that the local invasion of cancer cells might depend on the invasion ability of CAFs (CAFs-dependent cancer cell invasion) (Neri et al. 2015). The well-known types of cancer cell invasions include EMT (Sleeman and Thiery 2011; Christiansen and Rajasekaran 2006; Tsuji et al. 2009), mesenchymal

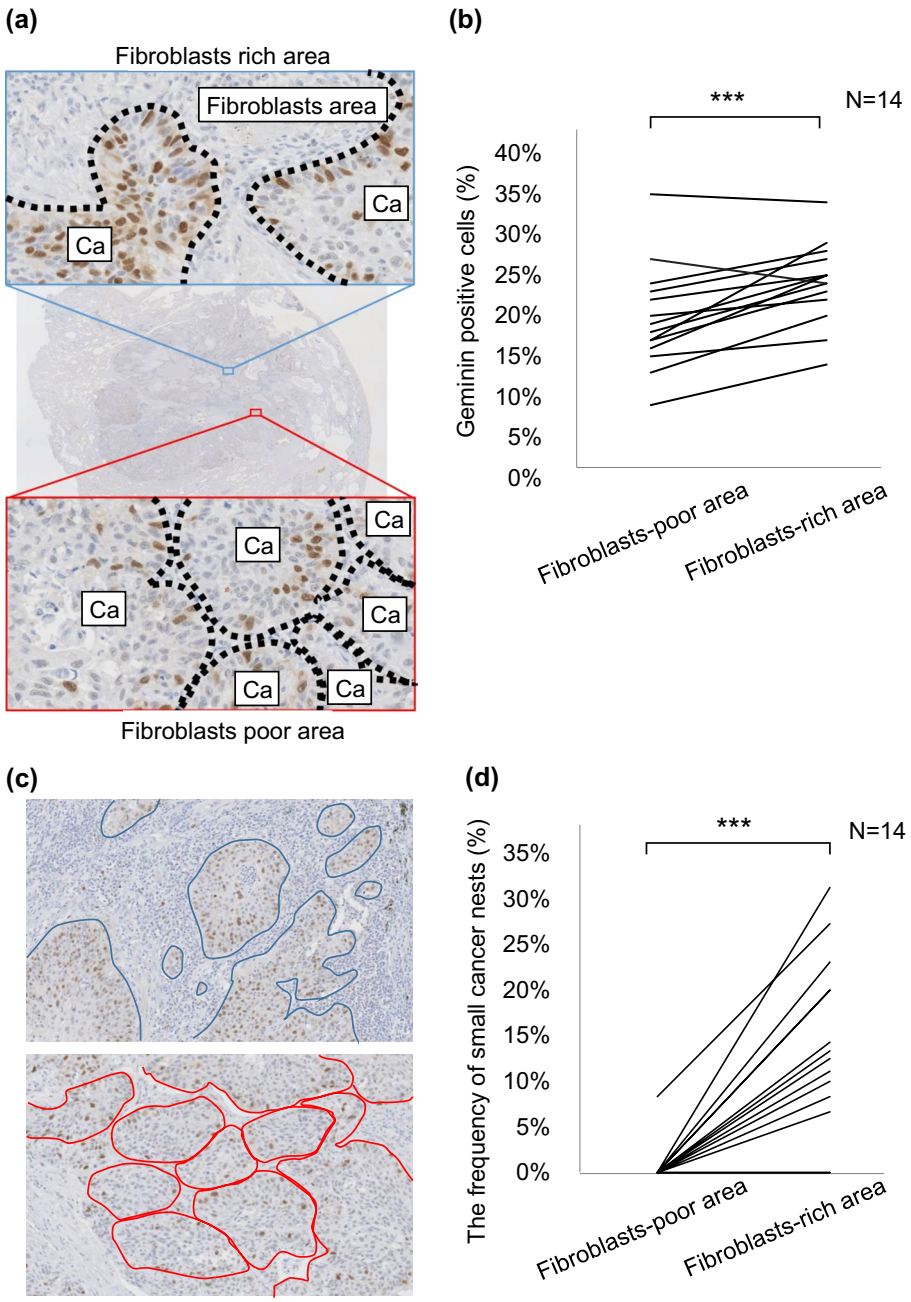

Fig. 6 Fibroblasts-poor area and fibroblasts -rich area in surgically resected squamous cell carcinoma tissue. **a** Representative image of geminin-positive cancer cells in fibroblasts-poor area (red line panel) and fibroblast-rich area (blue line panel). **b** The frequency of geminin-positive cells. Values are presented as mean of data of 14 patients. Statistical analysis was performed using Wilcoxon signed-rank test. ***$p < 0.01$. **c** Representative images of cancer nests in fibroblasts-poor area (red circle) and fibroblast-rich area (blue circle) (staining with geminin antibody). **d** The frequency of small cancer nests. Values are presented as mean of data of 14 patients. Statistical analysis was performed using Wilcoxon signed-rank test. ***$p < 0.01$

movement, which depends on MMPs secreted by cancer cells (Egeblad and Werb 2002; Wolf and Friedl 2011), and amoeboid movement, which upregulates their motor activity (Sanz-Moreno and Marshall 2010; Gao et al. 2017). In the current study, compared with the absence of fibroblasts, the total number of invaded A431 cells co-cultured with fibroblasts was significantly higher. We could not find any morphological changes of invaded cancer cells in fibroblast-dependent invasion area. So, it is unlikely that EMT occurs during fibroblast-dependent invasion. So, it is still unknown the relationship between EMT and fibroblast-dependent invasion manner. It is still unknown why cancer cells can more invade during fibroblast-dependent invasion process. Remodeled ECM by fibroblast may facilitate cancer cells to invade, alternatively, secretary factors from fibroblast may attract cancer cells. This would be a future study topic.

In the invasion area, the frequency of cancer cells in the S/G2/M phase was significantly higher when they were co-cultured with fibroblasts. This may be because the crosstalk between fibroblasts and A431 cells increases the proliferative activity of the cancer cells. In fact, when A431 cells and fibroblasts were co-cultured in a 2D model, this phenomenon could be detected (see Supplemental Fig. 3). Moreover, these in vitro results were confirmed in an in vivo situation

by analyzing surgically resected squamous cell carcinoma tissues. The local invasion of cancer cells may be potentiated by the higher proliferation activity that cancer cells acquire via crosstalk with fibroblasts.

Our in vitro study explored how A431 cells co-cultured with fibroblasts exhibited the formation of small cancer cell nests (type B and type C); however, these were not found in the absence of fibroblasts. This phenomenon was also confirmed in human squamous cell carcinoma samples. Although the exact molecular mechanism of how fibroblasts can influence the morphology of cancer cell nests is not known. The adhesion strength of cancer cell–fibroblast and/or the adhesion strength of cancer cell–matrix secreted from fibroblasts, may be the morphogenic regulator of small cancer cell nest (Labernadie et al. 2017).

In this study, we found that fibroblasts-dependent cancer cell invasion was characterized by the formation of small cancer cell nests and progression of cell cycle using both in vitro invasion assay and surgically resected specimens. These results would indicate biological differences between a fibrous tumor microenvironment and a non-fibrous tumor microenvironment. For the development of novel therapeutic strategies, understanding microenvironmental heterogeneity is of utmost importance.

Acknowledgements This work was supported in part by the National Cancer Center Research and Development Fund (23-A-12), and JSPS KAKENHI (24659185 and 16H05311). Tomoyuki Miyashita and Genichiro Ishii designed the study; Tomoyuki Miyashita performed in vitro experiments and analyzed the data; Tomokazu Omori, Hiroshi Nakamura, Masahiro Tsuboi, Masato Sugano, Genichiro Ishii and Tomoyuki Miyashita analyzed clinical and pathological data; Shinya Neri and Hiroko Hashimoto, Satoshi Fujii and Atsushi Ochiai provided intellectual advice; Tomoyuki Miyashita, and Genichiro Ishii wrote the manuscript.

Compliance with ethical standards

Conflict of interest All authors declare that they have no conflict of interest.

Ethical approval All procedures performed in studies involving human participants were in accordance with the ethical standards of the institutional and/or national research committee and with the 1964 Helsinki Declaration and its later amendments or comparable ethical standards.

Informed consent Comprehensive informed consent was obtained from all individual participants included in the study.

References

Christiansen JJ, Rajasekaran AK (2006) Reassessing epithelial to mesenchymal transition as a prerequisite for carcinoma invasion and metastasis. Cancer Res 66:8319–8326

Clark AG, Vignjevic DM (2015) Modes of cancer cell invasion and the role of the microenvironment. Curr Opin Cell Biol 36:13–22

Egeblad M, Werb Z (2002) New functions for the matrix metalloproteinases in cancer progression. Nat Rev Cancer 2:161–174

Friedl P, Alexander S (2011) Cancer invasion and the microenvironment: plasticity and reciprocity. Cell 147:992–1009

Friedl P, Wolf K (2003) Tumour-cell invasion and migration diversity and escape mechanisms. Nat Rev Cancer 3:362–374

Friedl P, Wolf K (2009) Proteolytic interstitial cell migration: a five-step process. Cancer Metastasis Rev 28:129–135

Friedl P, Locker J, Sahai E, Segall JE (2012) Classifying collective cancer cell invasion. Nat Cell Biol 14:777–783

Funai K, Yokose T, Ishii G, Araki K, Yoshida J, Nishimura M, Nagai K, Nishiwaki Y, Ochiai A (2003) Clinicopathologic characteristics of peripheral squamous cell carcinoma of the lung. Am J Surg Pathol 27:978–984

Gaggioli C, Hooper S, Hidalgo-Carcedo C, Grosse R, Marshall JF, Harrington K, Sahai E (2007) Fibroblast-led collective invasion of carcinoma cells with differing roles for RhoGTPases in leading and following cells. Nat Cell Biol 9:1392–1400

Gao Y, Wang Z, Hao Q, Li W, Xu Y, Zhang J, Zhang W, Wang S, Liu S, Li M, Xue X, Zhang W, Zhang C, Zhang Y (2017) Loss of ERalpha induces amoeboid-like migration of breast cancer cells by downregulating vinculin. Nat Commun 8:14483

Ishii G, Ochiai A, Neri S (2016) Phenotypic and functional heterogeneity of cancer-associated fibroblast within the tumor microenvironment. Adv Drug Deliv Rev 99:186–196

Kalluri R, Zeisberg M (2006) Fibroblasts in cancer. Nat Rev Cancer 6:392–401

Khalil AA, Friedl P (2010) Determinants of leader cells in collective cell migration. Integr Biol (Camb) 2:568–574

Konen J, Summerbell E, Dwivedi B, Galior K, Hou Y, Rusnak L, Chen A, Saltz J, Zhou W, Boise LH, Vertino P, Cooper L, Salaita K, Kowalski J, Marcus AI (2017) Image-guided genomics of phenotypically heterogeneous populations reveals vascular signalling during symbiotic collective cancer invasion. Nat Commun 8:15078

Labernadie A, Kato T, Brugues A, Serra-Picamal X, Derzsi S, Arwert E, Weston A, Gonzalez-Tarrago V, Elosegui-Artola A, Albertazzi L, Alcaraz J, Roca-Cusachs P, Sahai E, Trepat X (2017) A mechanically active heterotypic E-cadherin/N-cadherin adhesion enables fibroblasts to drive cancer cell invasion. Nat Cell Biol 19:224–237

Lammermann T, Sixt M (2009) Mechanical modes of 'amoeboid' cell migration. Curr Opin Cell Biol 21:636–644

Madsen CD, Sahai E (2010) Cancer dissemination–lessons from leukocytes. Dev Cell 19:13–26

Miyashita T, Higuchi Y, Kojima M, Ochiai A, Ishii G (2017) Single cell time-lapse analysis reveals that podoplanin enhances cell survival and colony formation capacity of squamous cell carcinoma cells. Sci Rep 7:39971

Neri S, Ishii G, Hashimoto H, Kuwata T, Nagai K, Date H, Ochiai A (2015) Podoplanin-expressing cancer-associated fibroblasts lead and enhance the local invasion of cancer cells in lung adenocarcinoma. Int J Cancer 137:784–796

Neri S, Hashimoto H, Kii H, Watanabe H, Masutomi K, Kuwata T, Date H, Tsuboi M, Goto K, Ochiai A, Ishii G (2016) Cancer cell invasion driven by extracellular matrix remodeling is dependent on the properties of cancer-associated fibroblasts. J Cancer Res Clin Oncol 142:437–446

Neri S, Miyashita T, Hashimoto H, Suda Y, Ishibashi M, Kii H, Watanabe H, Kuwata T, Tsuboi M, Goto K, Menju T, Sonobe M, Date H, Ochiai A, Ishii G (2017) Fibroblast-led cancer cell invasion is activated by epithelial-mesenchymal transition through platelet-derived growth factor BB secretion of lung adenocarcinoma. Cancer Lett 395:20–30

Sahai E (2007) Illuminating the metastatic process. Nat Rev Cancer 7:737–749

Sakaue-Sawano A, Kobayashi T, Ohtawa K, Miyawaki A (2011) Drug-induced cell cycle modulation leading to cell-cycle arrest, nuclear mis-segregation, or endoreplication. BMC Cell Biol 12:2

Sanz-Moreno V, Marshall CJ (2010) The plasticity of cytoskeletal dynamics underlying neoplastic cell migration. Curr Opin Cell Biol 22:690–696

Sanz-Moreno V, Gadea G, Ahn J, Paterson H, Marra P, Pinner S, Sahai E, Marshall CJ (2008) Rac activation and inactivation control plasticity of tumor cell movement. Cell 135:510–523

Schroeder A, Heller DA, Winslow MM, Dahlman JE, Pratt GW, Langer R, Jacks T, Anderson DG (2011) Treating metastatic cancer with nanotechnology. Nat Rev Cancer 12:39–50

Skhinas JN, Cox TR (2017) The interplay between extracellular matrix remodelling and kinase signalling in cancer progression and metastasis. Cell Adh Migr 1–9

Sleeman JP, Thiery JP: SnapShot (2011) The epithelial-mesenchymal transition. Cell 145:162 e1

Tsuji T, Ibaragi S, Hu GF (2009) Epithelial-mesenchymal transition and cell cooperativity in metastasis. Cancer Res 69:7135–7139

Wolf K, Friedl P (2011) Extracellular matrix determinants of proteolytic and non-proteolytic cell migration. Trends Cell Biol 21:736–744

Wolf K, Muller R, Borgmann S, Brocker EB, Friedl P (2003) Amoeboid shape change and contact guidance: T-lymphocyte crawling through fibrillar collagen is independent of matrix remodeling by MMPs and other proteases. Blood 102:3262–3269

Wolf K, Wu YI, Liu Y, Geiger J, Tam E, Overall C, Stack MS, Friedl P (2007) Multi-step pericellular proteolysis controls the transition from individual to collective cancer cell invasion. Nat Cell Biol 9:893–904